Predictions for the energy loss of light ions in laser-generated plasmas at low and medium velocities

W. Cayzac,[1,*] V. Bagnoud,[2,3] M. M. Basko,[4] A. Blažević,[2,3] A. Frank,[3] D. O. Gericke,[5] L. Hallo,[6] G. Malka,[1] A. Ortner,[7] An. Tauschwitz,[8] J. Vorberger,[9] and M. Roth[7]

[1]*Université Bordeaux-CEA-CNRS, Centre Lasers Intenses et Applications, UMR 5107, 33405 Talence, France*

[2]*GSI Helmholtzzentrum für Schwerionenforschung GmbH, Planckstr. 1, 64291 Darmstadt, Germany*

[3]*Helmholtz-Institut Jena, Fröbelstieg 3, 07743 Jena, Germany*

[4]*Keldysh Institute of Applied Mathematics (KIAM), Miusskaya sq. 4, 125047 Moscow, Russia*

[5]*Centre for Fusion, Space and Astrophysics, Department of Physics, University of Warwick, Coventry CV4 7AL, United Kingdom*

[6]*CEA-Cesta, 15 Avenue des Sablières BP2, CS 60001, 33116, Le Barp, France*

[7]*Institut für Kernphysik, Technische Universität Darmstadt, Schlossgartenstr. 9, 64289 Darmstadt, Germany*

[8]*Goethe-Universität Frankfurt am Main, Max-von-Laue-Str. 1, 60438 Frankfurt am Main, Germany*

[9]*Max-Planck Institute for the Physics of complex systems, Nöthnitzer Str. 38, 01187 Dresden, Germany*

(Received 30 April 2015; revised manuscript received 8 September 2015; published 24 November 2015)

The energy loss of light ions in dense plasmas is investigated with special focus on low to medium projectile energies, i.e., at velocities where the maximum of the stopping power occurs. In this region, exceptionally large theoretical uncertainties remain and no conclusive experimental data are available. We perform simulations of beam-plasma configurations well suited for an experimental test of ion energy loss in highly ionized, laser-generated carbon plasmas. The plasma parameters are extracted from two-dimensional hydrodynamic simulations, and a Monte Carlo calculation of the charge-state distribution of the projectile ion beam determines the dynamics of the ion charge state over the whole plasma profile. We show that the discrepancies in the energy loss predicted by different theoretical models are as high as 20–30%, making these theories well distinguishable in suitable experiments.

DOI: 10.1103/PhysRevE.92.053109 PACS number(s): 52.40.Mj

I. INTRODUCTION

The energy loss of ions in matter has been investigated for more than one century, raising considerable interest in various scientific fields (see, e.g., Ref. [1] for a summary) and finding concrete societal applications as, e.g., in tumor therapy [2]. The first theoretical treatments were the classical approach by Bohr [3], followed by the quantum-mechanical, but perturbative, calculations by Bethe and Bloch for the high-velocity behavior of light ions [4,5]. Later, more elaborate approaches beyond the perturbation theory were developed to extend the description to heavier ions with higher charges and lower velocities [6–10]. By now ion stopping in cold matter is relatively well understood, comprehensive reviews being, e.g., Refs. [1,11]. It has been characterized with abundant experimental data, most of which are compiled in Ref. [12], and several codes are available for routine calculations [13]. Due to various theoretical and experimental challenges, ion stopping in ionized matter is, in contrast, far from being understood. Moreover, only few experimental data have been collected. However, the localized heating of plasmas with ion beams [14–16] and, in particular, the diagnostics of plasmas with ions [17] are arising applications that require a good understanding of the beam-plasma interaction. Other applications are in the fields of high-energy-density physics [18], accelerator physics [19], and astrophysics [20,21].

Foremost, ion stopping in dense plasmas turns out to be a crucial aspect in the development of the inertial confinement fusion (ICF) concept. Here the major issue related to the energy deposition of ions is the precise description of the α-particle heating in the igniting and burning deuterium-tritium (DT) pellet. Efficient energy coupling determines the properties of the burn wave, the overall yield, and, thus, the success of a thermonuclear fusion experiment to a large extent [22–25]. In addition, all ICF schemes using ion beams as the main driver [14,26] or fast ignition by means of proton or carbon ion beams [27,28] also require a precise knowledge of the ion-stopping mechanisms in plasma.

The key physical quantity that determines the energy loss of the beam particles is the stopping power $-\frac{dE}{dx}$, defined as the ion energy deposited per unit length in the target. Similarly to the cold-matter case, the largest complication in the description of the ion stopping in plasma arises in the intermediate-velocity region where the stopping power has a maximum, which is reached when the projectile velocity v_b is close to the mean velocity of the target electrons. This maximum gives rise to the Bragg peak in the ion-energy deposition curve in matter and has thus a considerable influence on the whole stopping process and penetration range in the target. In cold matter, the maximum is reached when v_b is comparable to the velocity of the bound target electrons in a classical picture (a few times the Bohr velocity v_0), which corresponds to a projectile energy E_b of a few hundred keV/nucleon [29]. Although the stopping power far above this maximum ($E_b >$ 1 MeV/nucleon) is known with an accuracy of a few percentages, uncertainties of the order of 10% are reported close to the maximum [13]. The maximum of the stopping power in plasmas is reached when v_b matches the thermal velocity of the plasma electrons $v_{\mathrm{th}} = \sqrt{\frac{3k_B T_e}{m_e}}$. This maximum in $-\frac{dE}{dx}$ is even less understood for plasmas, as theoretical predictions show uncertainties of up to 50% depending on the projectile and plasma properties [30,31]. Until now, experimental data are scarce because measurements are extremely challenging.

*witold.cayzac@cea.fr

A. Parameters of the beam-plasma interaction

In the following we consider a beam of projectile ions with a velocity v_b and a charge state Z_b that interact with a plasma with an electron temperature T_e, an ion density n_i, an ionization degree Z_T, and, thus, a free-electron density $n_e = Z_T n_i$. The plasma can be characterized by two dimensionless parameters: the nonideality or Coulomb coupling parameter Γ and the degeneracy parameter Θ, defined by

$$\Gamma = \frac{e^2}{a_e k_B T_e} \quad \text{and} \quad \Theta = \frac{k_B T_e}{E_F}. \tag{1}$$

Here $a_e = (\frac{4\pi n_e}{3})^{-\frac{1}{3}}$ is the average distance between the electrons and E_F is the Fermi energy of the free electron gas in the target. While Γ gives an estimate for the coupling strength of the electrons, Θ quantifies the influence of the Pauli exclusion principle on the electron statistics.

Except for very small projectile velocities or very hot plasmas, the beam particles are much faster than the ions in the plasma and $v_b \gg v_{thi}$ holds. Here, $v_{thi} = \sqrt{\frac{3k_B T_e}{m_i}}$ is the thermal velocity of the plasma ions with mass m_i. In this regime, the contribution of the plasma ions to the stopping power can be neglected, hence only the electronic contribution needs to be taken into account (see, e.g., Ref. [32]).

Within a classical picture, the theoretical description of the stopping power depends essentially on the concerned impact parameter interval of the encounters between the projectile ions and the plasma electrons. A useful parameter to separate the contributions of different impact parameters is the screening length of the projectile moving in the plasma $\lambda = \lambda(v_b)$. Collisions with impact parameters $b > \lambda$ yield only small contributions to the stopping power as the field of the projectile is strongly screened. However, the excitation of collective plasma waves (plasmons) needs to be accounted for in this regime as well. Coulomb collisions with $b \sim \lambda$ are related to small-angle scattering (a Born or Fokker-Planck description is appropriate). Large-angle Coulomb scattering or close collisions occur for $b < \lambda$ and are especially important in dense plasmas. The relative importance of the different processes depends notably on the velocity ratio $\frac{v_b}{v_{th}}$ and is usually quantified by the Coulomb logarithm $\ln \Lambda = \ln(\frac{b_{max}}{b_{min}})$, where b_{min} and b_{max} are cutoff parameters (see, e.g., Ref. [33] for a discussion).

Another important quantity to be considered is the strength of the interaction between beam and plasma particles. It is often expressed by the Coulomb parameter η as introduced by Bohr [34] and discussed extensively in, e.g., Ref. [35],

$$\eta = \frac{Z_b e^2}{\hbar v_r}, \tag{2}$$

where v_r is the (average) relative velocity of the projectile-electron system. When $\eta \ll 1$, the interaction is weak compared to the relative kinetic energy. In this case, the first Born approximation is valid and a perturbative theory can be applied. Moreover, it should be noted that for $\eta \ll 1$ a quantum-mechanical treatment is required as quantum diffraction becomes important. In contrast, the beam ion-plasma coupling is strong for $\eta \geqslant 1$ and a nonperturbative description needs to be used. However, the stopping power can here be described classically if the target is nondegenerate.

As long as $v_b \gg v_{th}$, $\eta \ll 1$ holds if Z_b is not too large. Hence, the perturbation is small and the beam particles and the plasma are weakly coupled, i.e., a linear response treatment is appropriate, and the ion stopping power can be described within a first Born approximation for the scattering process of beam and plasma particles. Most of the ion energy-loss experiments in plasma have been carried out at $v_b \gg v_{th}$, hence in the linear regime [36–39]. Due to the high beam velocity, the experimental data can be interpreted in the frame of the widely used standard stopping model (SSM) [40] or, alternatively, of the random phase approximation (RPA) description [41]. This also includes the recent measurements of Ref. [42], with protons at 14 MeV energy probing a warm dense matter sample. Because $\frac{v_b}{v_{th}} \approx 13$, the target electron motion can be ignored and the beam-plasma interaction does belong to the linear regime, even if the target response is complicated due to coupling and degeneracy.

The theoretical modeling of the stopping power in the velocity domain of its maximum, for $v_b \approx v_{th}$, is much more difficult than in the perturbative region with $v_b \gg v_{th}$. Here the interaction between beam ions and plasma electrons can be strong, giving rise to numerous close collisions. Moreover, collective plasma oscillations (plasmons) can already be excited by the energetic ions. Due to strong Coulomb coupling, the first-Born approximation becomes questionable and nonperturbative approaches are required, especially in dense plasmas where large-angle collisions become important. Meanwhile, classical descriptions based on a binary-collision approach (see, e.g., Ref. [35]) are valid beyond the first-Born approximation, but they ignore dynamic effects like the excitation of plasma waves. A unified approach is possible in the framework of quantum kinetic theory [30,84]. Nevertheless, a complete description of the stopping power in the intermediate velocity range where the stopping maximum is reached has not been achieved yet. Accordingly, large discrepancies exist between the various theories [30,31,43].

However, a benchmarking of the theories in that low-velocity region is crucial for the applications mentioned above and especially for the α-particle heating in ICF where a major part of the interaction takes place for $v_b \leqslant v_{th}$. As recently highlighted by experiments at the National Ignition Facility, the understanding of the α-particle heating is one of the major issues to be solved in order to achieve ignition [44,45]. By now the scarce available experimental data close to the maximum of the stopping power [46,47] have not enabled us to benchmark the theoretical predictions due to incompletely known projectile or plasma parameters.

The present work fits into the project of performing energy-loss measurements at GSI Helmholtzzentrum für Schwerionenforschung in Darmstadt, Germany. It considers a well-characterized beam-plasma configuration that is suited for a first-time test of the stopping-power theories at the maximum of the stopping power, which is reached in the regime of low beam velocity. As a preliminary step to the experiments, this paper presents the corresponding theory and simulation results, considering light projectile ions with the example of carbon, interacting with a hot laser-induced plasma. Our main goal is to determine the differences between theories

and, thus, define the experimental requirements to benchmark these models. Our results show that discrepancies of up to 30% can be expected between the predictions of different energy loss theories in this configuration, making it a well-suited test bed for benchmarking and defining the experimental energy resolution required.

Section II presents the simulation of the experiments that are being planned at GSI. The hydrodynamic simulations of the laser-induced plasma and the Monte Carlo calculations of the beam charge-state distribution are addressed. Section III presents the corresponding stopping-power and energy-loss predictions, with a comparative study of different perturbative and nonperturbative theories. Section IV discusses the details and the relevance of the used stopping-power theories and models. Section V gives a conclusion and summary.

II. SIMULATION OF AN EXPERIMENT

The recent progress in ion-stopping experiments at GSI enables an investigation of the ion energy loss in a laser-generated plasma at low projectile velocities, where the stopping-power maximum is reached.

A beam-plasma configuration consisting of light projectile ions probing a highly ionized carbon plasma around the stopping-power maximum is considered. Two-dimensional (2D) hydrodynamic simulations of the plasma evolution as well as Monte Carlo calculations of the charge-state distribution of the ion beam in the plasma give access to the whole interaction conditions as a function of space and time. This will allow to determine the stopping-power profiles of the ions in the plasma as well as the resulting energy loss of the beam.

A. Plasma target

The studied plasma is generated by the irradiation of a 100 μg/cm^2 planar graphite foil by two laser beams from opposite sides [39]. Both beams are frequency doubled (2ω) with wavelengths of 527 nm and 532 nm, an energy of 30 J, and a pulse length of 7 ns at full width at half maximum (FWHM). The beams are spatially smoothed by using random phase plates (RPP) [48], which create a top-hat focus profile with a 1-mm diameter on the target. The plasma parameters are obtained from hydrodynamic-simulation data with the two-dimensional radiative RALEF2D code [49,50]. The schematics of the setup used for the modeling is represented in Fig. 1 together with the radial and temporal laser-beam profiles used as input. This plasma target has been used in a previous work for energy-loss measurements with an argon beam at a projectile energy $E_b = 4$ MeV/nucleon [39], in which case $\frac{v_b}{v_{\rm th}} \approx 4$ and the experimental data could be well explained by using a specifically modified version of the CASP code to account for the various electronic shell contributions [9].

The RALEF2D code uses an arbitrary Lagrangian-Eulerian method for the mesh evolution and a second-order Godunov scheme for the numerical resolution of the plasma fluid equations. It is based on a one-fluid and one-temperature hydrodynamic model and considers heat conduction as well as radiative transport in its description of the plasma heating. For this purpose, the hydrodynamic evolution is coupled with the solution of the equation of frequency-dependent

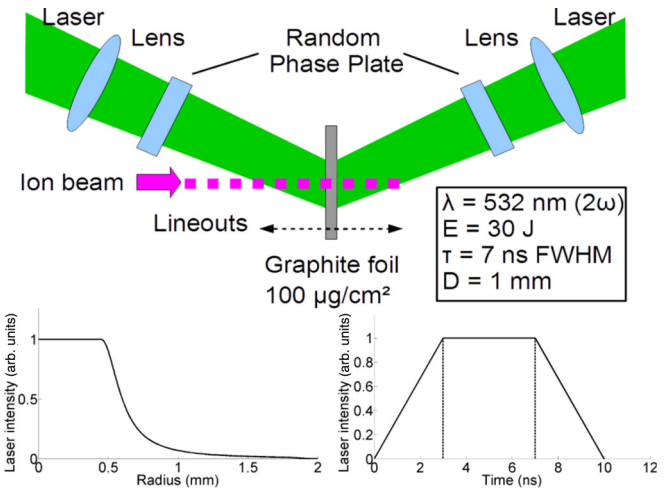

FIG. 1. (Color online) Schematics of the plasma simulation setup with the radial and temporal laser-beam profiles. Parameter lineouts as shown in following graphs are directed along the ion propagation axis as indicated.

radiative transport in the quasistatic approximation. The precise description of radiative transport is a key point as the dynamics of hot laser-generated plasmas is strongly influenced by radiative phenomena.

The simulated density and temperature profiles are the same as those used in Ref. [39]. In the latter work, the plasma ionization distribution was described with the help of the Saha equation by using an iterative algorithm [51]. Here, a more elaborate ionization equation of state (EOS) is used instead [52], still in the frame of the local thermodynamical equilibrium (LTE) hypothesis.

The predictions of the RALEF2D code have been validated by plasma free-electron density measurements using multiframe laser interferometry [53]. The radial density profiles have been compared in the low density domain with $n_e \approx 10^{19}$–10^{20} cm^{-3}, and an agreement better than 20% has been found between the measured and the simulated profiles. This shows the reliability of the simulation and justifies the use of the obtained parameter profiles including the denser plasma parts. The laser and target parameters are tailored to obtain a fully ionized carbon plasma after 6–7 ns of laser irradiation. This can be seen in Fig. 2, where the temporal evolution of the

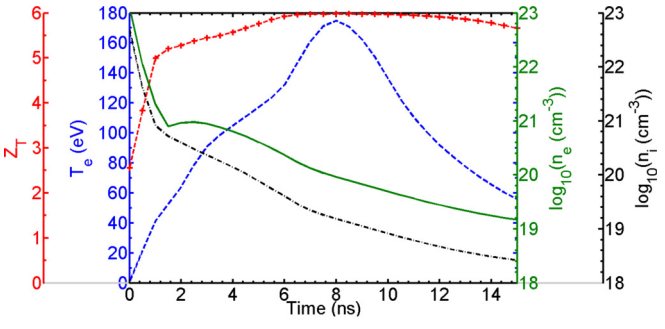

FIG. 2. (Color online) Profiles of the plasma free-electron density (plain line), ion density (dash-dotted line), electron temperature (dashed line), and ionization degree (dashed line with crosses) in the target center and averaged over the ion axis as a function of time.

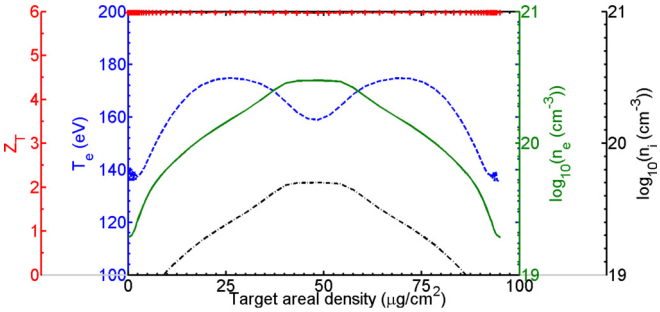

FIG. 3. (Color online) Profiles of the plasma free-electron density (plain line), ion density (dash-dotted line), electron temperature (dashed line), and mean ionization degree (dashed line with crosses) as a function of the target areal density along the ion propagation path in the target center at $t = 7$ ns after laser impact.

plasma parameters at the target center (averaged over the ion propagation axis) is represented.

The plasma reaches a maximum electron density of $n_e \approx 5 \times 10^{20}$ cm^{-3} (when fully ionized) and a maximum electron temperature of $T_e \approx 180$ eV, which corresponds to an ideal and nondegenerate plasma with $\Gamma \approx 0.01$ and $\Theta > 500$. The full ionization of the plasma is visible in a time window of $t = 6$–12 ns after the beginning of the laser heating of the target. At later times, the plasma cools down and Z_T slowly decreases. Besides it can be seen that before $t = 2$ ns the used EOS overevaluates the ionization degree.

The randomized, two-sided irradiation with frequency-doubled laser light and the subsequent rapid radiation transport in the target result in well-reproducible and quite homogeneous plasma conditions. The longitudinal gradients of the plasma parameters are shown in Fig. 3 at $t = 7$ ns, in the target center along the ion propagation axis as a function of the target areal density $l(x) = \int_0^x \rho(x')dx'$, where $\rho(x')$ is the target mass density. The areal density, though not corresponding to a linear length coordinate, is the relevant abscissa coordinate for an energy-loss calculation.

When propagating through the target at that time, the ions interact with a uniformly fully ionized plasma that features a certain gradient in T_e and n_e. As is shown later, in spite of these longitudinal gradients, the stopping power along the trajectory through the target is nearly constant.

Transversally to the ion axis, the plasma has been made as uniform as possible by using the 1-mm smoothed focus profile. As a consequence, as long as the diameter of the probing ion beam remains below 1 mm, all the projectile ions are expected to interact with a quasiuniform hot and highly ionized plasma volume. In Ref. [39], the beam was reduced to a 0.5-mm diameter by a pinhole before the interaction with plasma. In this way the plasma appeared nearly one dimensional for the incoming ions. Another advantage of this irradiation scheme is that the plasma expands one dimensionally along the ion axis roughly in the first 7 ns of the interaction, thus keeping a stable target areal density.

B. Projectile ion beam

Knowing the value of $v_{\text{th}} \approx 10^7$ m/s in the hot and highly ionized plasma region, a projectile energy of 0.5 MeV/nucleon is required to probe the plasma at the maximum of the stopping power. Describing the projectile charge state in a plasma is a complex issue because, in contrast to cold targets, the charge equilibrium is not necessarily reached. The uncertainties related to the projectile charge-state value in a plasma have often prevented a reliable interpretation of experimental data as in, e.g., Refs. [38,46]. Around the stopping-power maximum the situation is even more complicated due to expected strong nonequilibrium charge-state behaviors [54] and multiple charge-exchange processes due to the strong beam-plasma coupling [55].

This is why a key requirement of the described setup is to simplify the projectile charge-state distribution as much as possible. For this purpose, a light-ion beam is considered that is expected to become highly stripped in the fully ionized carbon plasma due to the strong reduction of the nonradiative electron capture (NREC) cross section. In the following, we consider carbon projectiles as the lightest ions available experimentally. The charge-state distribution of a carbon ion beam in the plasma was computed by using a Monte Carlo simulation of the charge-exchange processes [56–58]. The cross sections for projectile ionization and excitation on target ions as well as for NREC and radiative electron capture (REC) are obtained from the ETACHA code [59]. They are calculated in a plane-wave Born approximation [60], an eikonal approximation [61], and by the Bethe-Salpether formula, respectively [62], and the screening properties of the target are specifically modified to describe the plasma state. For the mechanisms involving free electrons and thus specific to plasma, the cross sections for impact electron ionization were taken from Ref. [63], the ones for dielectronic recombination come from the model of Ref. [54], and the ones of three-body recombination are as described in Ref. [64].

The calculations consider a number of 10^5 ions with an initial projectile charge state of 4+, which is closest to the equilibrium charge-state value of carbon ions in a solid carbon target at $E_b = 0.5$ MeV/nucleon [65]. The obtained charge-state distribution of the carbon beam in the plasma is shown in Fig. 4 at $t = 7$ ns, again in the target center along the ion propagation path as a function of the target areal density. The

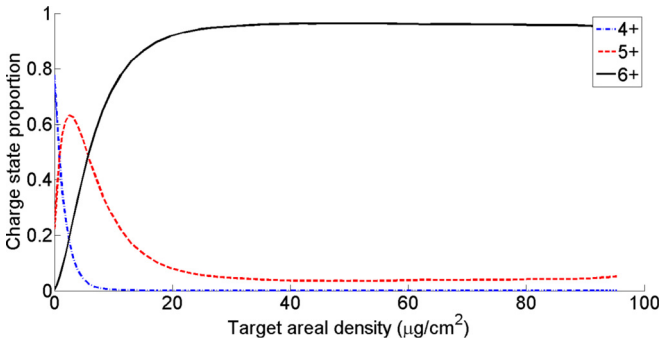

FIG. 4. (Color online) Charge-state fractions of a carbon ion beam as a function of the target areal density along the ion propagation path in the target center at $t = 7$ ns after laser impact for the plasma parameters of Fig. 3. The projectile ions penetrate the plasma from the left side with an initial charge of 4+. Note that for an increased accuracy, the shown distribution still needs a corrective scaling (see text).

results show that the beam, entering the target from the left side with an initial charge state 4+, reaches a charge equilibrium with about 96 % of the ions in the state 6+ after propagating through around 20 $\mu g/cm^2$ within the plasma target.

For C^{6+} projectile ions interacting at a 0.5-MeV/nucleon energy in the plasma, the Coulomb parameter verifies $\eta \approx 1.1$. Hence, the perturbation induced on the plasma electrons is important and the weak-coupling stopping-power approaches are questionable. Furthermore, it can be estimated using, e.g., Refs. [32,66] that the contribution of the collective plasma effects to the stopping power reaches approximately 10% even at this low projectile velocity. Therefore the stopping-power description needs to consider close collisions as well as dynamic plasma effects and it requires a priori a nonperturbative approach.

However, the charge-transfer cross sections used in the Monte Carlo code are mainly based on perturbative methods. Therefore, for a more reliable charge-state calculation, the cross sections obtained with the ETACHA code need to be benchmarked and scaled with experimental data. This calibration process can be carried out with the help of measurements of nonequilibrium beam charge-state distributions exiting solid target foils [56,67]. Then, by fitting the charge fractions to the data, an absolute determination of the charge-transfer cross sections is possible. In this way a corrective scaling of the simulated charge-state distributions can be obtained, which is also used in the plasma case. Existing charge-state data in cold matter [68] show that for an energy of 0.5 MeV/nucleon the charge equilibrium for light ions is reached after around 5–10 $\mu g/cm^2$ foil thickness. Hence, for the code calibration, charge-state-distribution measurements have to be performed for a foil thickness interval below 10 $\mu g/cm^2$.

III. ION-STOPPING CALCULATIONS

A. Stopping power

The predictions of several stopping-power theories are shown in Fig. 5 on the example of a C^{6+} projectile ion in a fully ionized C plasma for typical parameters of $n_e = 5 \times 10^{20}$ cm^{-3} and $T_e = 150$ eV as a function of the projectile energy.

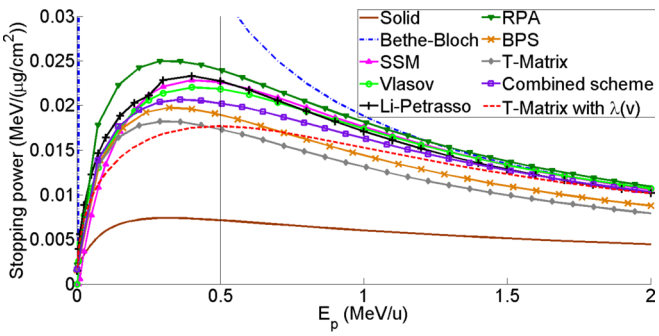

FIG. 5. (Color online) Comparison of the stopping power of C^{6+} ions in a fully ionized plasma with $n_e = 5 \times 10^{20}$ cm^{-3} and $T_e = 150$ eV as predicted by different theories as a function of the projectile energy E_b. The stopping power in solid carbon is shown for comparison. The vertical bar indicates the initial projectile energy of 0.5 MeV/nucleon.

In Fig. 5, the SSM [40], the RPA stopping power [30], another dielectric stopping power derived from the Vlasov equation [32], the Li-Petrasso stopping model [66], the Brown-Preston-Singleton (BPS) stopping power [85], as well as the Bethe-Bloch formula are perturbative approaches, while the T matrix [30] and the T matrix with $\lambda(v)$ [31,69] schemes as well as the combined scheme [30] stand for nonperturbative calculations. The details of these theories will be discussed in Sec. IV. The stopping power in solid carbon is also plotted for comparison, as taken from the SRIM tables [70].

The graph interestingly shows that the stopping-power maximum in the plasma for this temperature is reached at almost the same energy as in the solid, and a stopping-power increase of about 200–300% is expected in the plasma at $E_b =$ 0.5 MeV/nucleon for these plasma parameters. Furthermore, for sufficiently high projectile energies (from approximately 2 MeV/nucleon) most of the theories for plasma are consistent, reaching the Bethe limit, with the exception of the T-matrix and of the BPS approaches. Meanwhile, for energies below 2 MeV/nucleon all theories start differentiating from each other, and the discrepancies culminate at the stopping-power maximum. Close to this maximum, most linear approaches (RPA, SSM, Vlasov, Li-Petrasso) make quite similar predictions, while the Bethe-Bloch formula significantly overevaluates the stopping power and the BPS theory predicts 20% smaller values. In contrast, the nonperturbative T-matrix schemes predict a 30% smaller stopping power than most of the perturbative approaches and the combined scheme about 10% smaller. This suggests that beam-plasma correlations due to strong projectile-electron coupling play a significant role in the interaction. The calculated discrepancies between the models remain important for a wide range of n_e and T_e as long as $T_e \geqslant 100$ eV, i.e., when the plasma is highly ionized.

B. Energy-loss calculations

The energy loss was calculated by combining the plasma simulation data obtained from the RALEF2D code with the Monte Carlo calculation results of the projectile charge-state distribution. For each time step of the hydrodynamic simulation, the stopping-power profile was determined along the plasma areal-density profile. The calculation was performed according to the SSM, Vlasov, Li-Petrasso, and Bethe-Bloch perturbative approaches as well as the nonperturbative T matrix with $\lambda(v)$ scheme considered in Sec. III A.

The used theories and models are valid for stopping by free electrons. For the time domains where the plasma is not fully ionized, the bound-electron contribution needs to be estimated, which is approximately done with the help of a corresponding Bethe formula. It turns out that the bound electron influence on the stopping power is only visible in the first nanoseconds of the interaction.

Another point to be considered is the reduction of the projectile energy along the propagation throughout the target. The energy exiting the plasma is indeed 10–20% smaller depending on the theory, and the velocity dependence of the stopping power thus has to be included. For the Bethe-Bloch formula the velocity variation is even larger due to its strongly increasing stopping-power values with decreasing velocity. This effect was taken into account by applying an Euler scheme

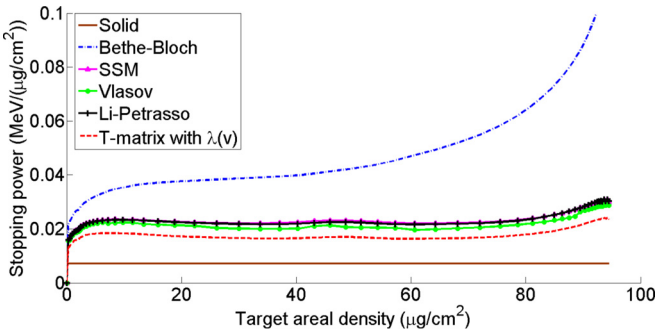

FIG. 6. (Color online) Calculated stopping-power profiles as a function of the target areal density along the ion propagation path in the target center at $t = 7$ ns after laser impact. The stopping-power in solid carbon is also plotted for comparison. The projectile ions penetrate the plasma from the left side.

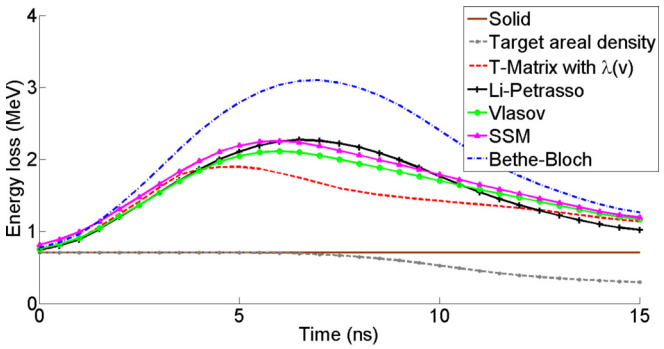

FIG. 7. (Color online) Energy loss as a function of time according to the considered theoretical stopping predictions. The energy loss in the solid target and the evolution of the plasma areal density are shown as reference curves.

to determine the actual stopping-power value at each point of the ion trajectory in the plasma.

The calculated stopping-power profiles are plotted in Fig. 6 at the time $t = 7$ ns on the ion axis as a function of the target areal density in the target center and thus they correspond to the plasma and beam parameters of Fig. 3 and Fig. 4. Apart from the Bethe-Bloch profile, the stopping-power curves remain at a stable level due to the nearly constant plasma and projectile ionization degree, while the gradients in T_e are smoothed in the stopping Coulomb logarithm.

The energy loss ΔE was calculated in 0.5-ns time steps between $t = 0$ and 15 ns by the integration of the stopping-power profiles as the one shown in Fig. 6, following

$$\Delta E = -\int \frac{\partial E}{\partial \rho x}(x)\rho(x)dx. \tag{3}$$

For a calculation in realistic experimental conditions, the spatial and temporal distributions of the ion beam were both described by Gaussian functions. First, the typical duration of 3 ns at FWHM of the ion bunches available for stopping experiments at GSI was considered by averaging the energy loss over different plasma profiles over time. Second, the calculation includes the effects of the transversal width of the ion beam (about 500 μm FWHM) by averaging the Gaussian ion beam distribution over the whole plasma profile, including the external regions where the plasma parameters somewhat differ and the target areal density is smaller than on the central axis. A number of 10^3 ions per bunch were simulated, which roughly corresponds to the expected experimental conditions.

The calculated energy loss is presented in Fig. 7 as a function of time, where the lasers start irradiating the target at $t = 0$ ns. Its value of 0.71 MeV in the solid target, as estimated with the SRIM code, is shown as a reference. The plasma areal density is plotted as an indicator of the plasma expansion.

The graph shows an energy-loss enhancement in the plasma due to the simultaneous increase in the projectile mean charge-state and of the stopping-power Coulomb-logarithm values, both due to the increasing ionization degree. A maximum is reached when the plasma becomes fully ionized and features its maximum temperature, which corresponds to the maximum of the stopping power with $\frac{v_b}{v_{th}} \approx 1$. The areal density stays constant during the first 6–7 ns of the 1D plasma-expansion phase, and later it decreases due to the 3D plasma expansion into vacuum. This effect as well as the steady reduction of the temperature and of the ionization degree at later times cause a subsequent decrease of the energy loss. The data show a maximum enhancement of 200% to 300% in relation to its value in solid carbon, in accordance with the predictions of Fig. 5.

One significant uncertainty on the energy-loss calculation comes from the choice of the ionization EOS. This is shown in Fig. 8, where the energy loss according to the T matrix with $\lambda(v)$ is compared for a plasma ionization distribution calculated according to (i) the Saha equation (in LTE), (ii) the LTE ionization EOS from Ref. [52] that has been used in the RALEF2D simulations, as well as (iii) the LTE and (iv) the non-LTE version of the FLYCHK code [71]. It appears that under the LTE assumption and especially when using the Saha equation, the plasma ionization degree is significantly higher in comparison with the non-LTE calculation. Hence assuming LTE, the free-electron density as well as the mean projectile charge state are in turn overevaluated. As a result, the energy loss predicted when using the non-LTE FLYCHK code is significantly smaller than with the LTE descriptions and especially the Saha equation. This effect is quite considerable

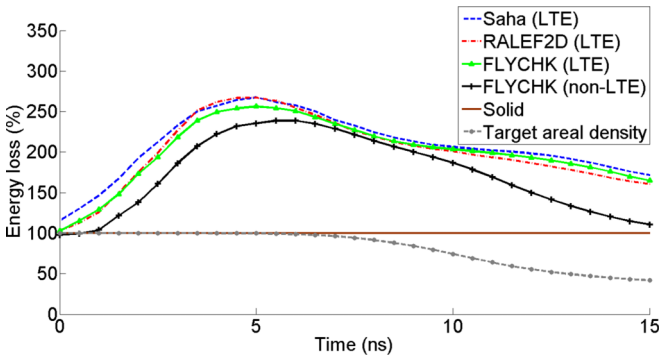

FIG. 8. (Color online) Energy loss in the target center, normalized to its value in the solid target, as a function of time according to the T matrix with $\lambda(v)$, with the plasma ionization calculated with the Saha equation, the LTE EOS from Ref. [52] used in this work, as well as with the LTE and non-LTE options of the FLYCHK code.

at early and late times, corresponding to $T_e \lesssim 100$ eV. In contrast, when T_e is highest, between $t = 6$ and 10 ns, the differences between the results are small. In particular, the use of the LTE descriptions causes a hump in the energy-loss curves after $t = 10$ ns by predicting a too-high ionization degree. Hence, due to the necessary LTE assumption for the plasma simulations, an error of up to 30% for $t < 6$ ns and $t > 10$ ns might affect the energy-loss calculation.

The energy-loss curves of Fig. 7 and Fig. 8 can be directly compared with experimental data. In order to meet the condition $\frac{v_b}{v_{\rm th}} \approx 1$ and thus for an optimal theory benchmarking, the measurements should be performed at times roughly between $t = 5$ and 10 ns after the start of the target heating. An energy resolution of 100 keV in the experiment would allow us to differentiate between all of the presented theories in that time domain, while a worse resolution of 300 keV would still allow to distinguish the T-matrix predictions from the perturbative results.

IV. DISCUSSION OF THE STOPPING-POWER APPROACHES

The available stopping-power theories are well suited in the case of $v_b \gg v_{\rm th}$, where most measurements were performed, but their reliability for $v_b \approx v_{\rm th}$ is questionable.

At high beam velocities, as long as the beam charge Z_b is not too large, the weak-coupling approximation holds and the interaction can be described, e.g., within a dielectric plasma theory. In that frame, the projectile potential generates a polarization of the medium that is described by means of a dielectric function, and the induced field counters the motion of the projectile. Different levels of approximation are possible for the dielectric function depending on the consideration of collisions and local field corrections. Applying the RPA in the general kinetic equation, the Lenard-Balescu collision integral [72,73] is obtained, leading to the so-called RPA stopping power [30,41,74,75]. Perturbative by nature, it is sometimes called the "Born-RPA" in the literature. In Sec. III, the RPA stopping power is implemented following the formula of Ref. [30]. An alternative dielectric expression can be derived from the linearized system of the Vlasov-Poisson equations [32], which is used in this work as the "Vlasov" stopping power. Dielectric descriptions take the contributions of small-angle collisions and of collective plasma oscillations into account, but they ignore close collisions. As they belong to the linear beam-plasma coupling regime, they are characterized by a Z_b^2 dependence of the stopping power. The choice of the dielectric function is important, as it is shown in Fig. 5 that the "Vlasov" stopping-power predictions lie 10–20% below the RPA ones around and below the maximum.

For very high beam velocities $v_b \gg v_{\rm th}$, the stopping power within the dielectric description reduces to the asymptotic Bethe-like formula [4]. Considering the contributions of free electrons in the plasma, one obtains

$$\left(\frac{\partial E}{\partial x}\right)_{\rm Bethe} = -\frac{Z_b^2 e^2 \omega_p^2}{v_b^2} \ln\left(\frac{2 m_e v_b^2}{\hbar \omega_p}\right), \tag{4}$$

where $\omega_p = \sqrt{\frac{4\pi n_e e^2}{m_e}}$ is the plasma frequency.

The first departures from the Bethe formula at lower beam velocities can be described via the Bloch and Barkas corrections. The Bloch correction $L_{\rm Bloch}$ [5] improves the treatment of close collisions that become increasingly important when v_b decreases. The Barkas correction $L_{\rm Barkas}$ [76] accounts for higher-order polarization, which notably explains why the stopping powers of positive and negative ions with the same absolute charge value differ. The resulting expression is usually called the SSM [40]. Despite the corrections, it remains a high-velocity approximation. In the present calculations the Bethe-Bloch formula has been applied for comparison purposes. Even if the close-collision contribution included in the Bloch correction leads to a reduction of the stopping power compared to the simple Bethe formula (4), the Bethe-Bloch expression appears to significantly overestimate the stopping power around its maximum. It can be noted that as the interaction takes place in the classical regime ($\eta \geqslant 1$), the Bethe-Bloch formula is equivalent here to the classical Bohr expression [3].

Stronger beam-plasma coupling can furthermore be included approximately with a thermal coupling factor $G(\frac{v_b}{v_{\rm th}})$ (Chandrasekhar function) [77]. This function also appears in the description of the stopping process in the Fokker-Planck approach and represents the projectile friction coefficient with respect to the Maxwellian plasma electron background. It can be combined with a dielectric expression [32] or the SSM as suggested in Ref. [46]. Considering all the corrections mentioned above, one obtains

$$\left(\frac{\partial E}{\partial x}\right)_{\rm SSM} = -\frac{Z_b^2 e^2 \omega_p^2}{v_b^2} G\left(\frac{v_b}{v_{\rm th}}\right) \times \left[\ln\left(\frac{2 m_e v_b^2}{\hbar \omega_p}\right) + L_{\rm Bloch} + Z_b L_{\rm Barkas}\right]. \tag{5}$$

The Barkas correction is proportional to Z_b^3 and the Bloch correction to Z_b^4. Therefore, these two corrections are mostly important for heavy ions, while for light ions as in our case the thermal correction is predominant. This SSM expression is implemented in the calculation but the Barkas term is omitted because it causes an unphysical peak at low energy, thus appearing not to be suited for this parameter region. In our case, the SSM with the Bloch and Chandrasekhar corrections produces very similar results to the dielectric approach derived from the Vlasov equation. Strictly speaking, the Bethe-Bloch formula and thus the SSM are not perturbative in lowest order only because they contain higher-order terms in Z_b and do not feature a strict Z_b^2 dependence of the stopping power. Though these terms, while allowing us to extend the description at lower velocities, remain *ad hoc* corrections which do not necessarily remain valid around the stopping-power maximum.

A more elaborate perturbative model for the stopping power was developed by Li and Petrasso by using a Fokker-Planck approach [66]. Here, all possible impact parameters are taken into account, though approximately. The expression is based on a Coulomb logarithm describing small-angle collisions, with the inclusion of an improved thermal coupling factor G with higher-order terms to account for close collisions. The weakness of the Fokker-Planck approach to not consider the collective behavior of the plasma was mitigated by artificially

adding a Bethe-like tail for high beam velocities:

$$\left(\frac{\partial E}{\partial x}\right)_{\text{Li-Petrasso}} = -\frac{Z_b^2 e^2 \omega_p^2}{v_b^2} G\left(\frac{v_b^2}{v_{\text{th}}^2}\right) \ln\left(\frac{b_{\max}}{b_{\min}}\right) + u\left(\frac{v_b}{v_{\text{th}}}\right) \ln\left(1.123\,\frac{v_b}{v_{\text{th}}}\right), \quad (6)$$

where u denotes the unit step function. The irregularity in the slope of the Li-Petrasso curve comes from the use of this step function. Although limited to the linear interaction regime, the Li-Petrasso stopping model has been widely used in ICF calculations (see, e.g., Ref. [78]). In our calculation, its predictions are almost identical to those of the "Vlasov" dielectric model and of the SSM. It shows that these models, despite some higher-order corrections, describe essentially the same physics on the linear interaction level.

The stopping power can also be evaluated on the basis of more elaborate kinetic equations. This includes nonperturbative treatments of the beam-plasma interaction that is particularly important around the maximum of the stopping power in velocity or energy space. Such theories have recently been developed to account for the strong beam-plasma correlations that arise in ICF situations, based on plasma kinetic theory [30,31,79,80]. In this work, approaches based on the T-matrix schemes of Ref. [30] and Refs. [31,69], stemming from quantum kinetic theory, are considered.

The T-matrix schemes are derived from a ladder approximation of the Boltzmann kinetic equation for binary collisions [81,82]. Due to the full consideration of all ladder terms (multiple scattering), they can describe effects of strong correlations and account for binary collisions of arbitrary strength. Accordingly, they are essentially nonlinear in the interaction strength. The T-matrix scheme of Ref. [30] considers a spherically symmetric, screened Coulomb potential of the projectile where screening is taken to be static. As a result, it ignores collective plasma effects and does not reach the Bethe limit at high velocity as shown in Fig. 5. In order to add the collective contributions associated with the excitations of plasmons and ensure the correct, Bethe-like high-velocity tail of the stopping power, a velocity-dependent screening length $\lambda(v_r)$ has been introduced [31,35,69], resulting in the "T matrix with $\lambda(v)$" scheme. It has been shown that the T-matrix approach using the velocity-dependent screening length $\lambda(v_r)$ agrees well with simulation results from particle-in-cell (PIC) and molecular dynamics (MD) codes [31,35]. A fit formula of the model [69] gives an accuracy of better than 25% for T_e below 400 eV and is used for the present calculation.

Alternatively, strong beam-plasma correlations and dynamic screening effects can be combined with the Gould-deWitt scheme first applied to the electrical conductivity [83]. This combined scheme adds the results according to the Boltzmann equation (strong correlations but static screening) and the Lenard-Balescu equation (dynamic screening but first-order Born approximation). The static first-order Born approximation has to be subtracted to avoid double counting of the first term of the ladder series. For the stopping power, we have [79,84]

$$\left(\frac{\partial E}{\partial x}\right)_{\text{comb}} = \left(\frac{\partial E}{\partial x}\right)_{\text{static}}^{\text{T matrix}} + \left(\frac{\partial E}{\partial x}\right)_{\text{dynamic}}^{\text{RPA}} - \left(\frac{\partial E}{\partial x}\right)_{\text{static}}^{\text{1st Born}}. \quad (7)$$

Here the T-matrix contribution accounts for close collisions and the RPA term includes effects of dynamic screening.

Another theory following the same Gould-deWitt idea uses a combination of the Lenard-Balescu and Boltzmann kinetic equations via dimensional continuation. This so-called BPS approach provides perturbative stopping results in highly ionized, ideal plasmas [85,86] and has been applied for ICF calculations as well [87,88].

A particularly interesting result of the nonperturbative approaches is the prediction of a weaker dependence of the stopping power on the projectile charge state, $\frac{dE}{dx} \propto Z_b^y$ with $y < 2$. It can be noted that a deviation from the perturbative Z_b^2 scaling is also found in stopping-power expressions resulting from classical binary-collision theory as in the Bohr formula, where $\frac{dE}{dx} \propto Z_b^2 \ln[\frac{f(n_e,T_e)}{Z_b}]$. Hence, the approaches containing T-matrix contributions predict a smaller stopping power than the linear approaches based on a first Born approximation (with the exception of the BPS calculation). These discrepancies increase with the beam-plasma coupling η. Depending on the beam and plasma parameters, the nonperturbative theories can predict the stopping power to be more than 50% smaller than the RPA approach around the maximum of the stopping power [30,31,69]. For the parameters considered in this work, as shown in Sec. III, the inclusion of the influence of close collisions and beam-plasma correlations, by weakening the Z_b dependence of the stopping power, leads to a considerable reduction, up to 30%, of the stopping power compared with most of the perturbative results.

V. SUMMARY AND CONCLUSION

The largest discrepancies between the existing ion stopping-power theories and models arise around the stopping-power maximum. Therefore, this parameter region requires most investigation, while also being the most relevant for a theory benchmarking with experimental data. Even if precise data relevant to ICF conditions still do not exist and measurements are very challenging, an experimental test of the stopping-power theories can be carried out in laser-induced plasmas at much smaller densities by using a low-velocity ion beam to probe the region of the stopping-power maximum.

For that purpose, a test bed for energy-loss measurements of light ions like carbon in a highly ionized laser-generated carbon plasma has been simulated. Data from hydrodynamic simulations of the plasma and from Monte Carlo calculations of the beam charge-state distribution have been combined in order to determine the predictions of various stopping-power theories and models. The comparison between perturbative and nonperturbative stopping-power approaches reveals discrepancies of up to 30%.

Energy-loss experiments are planned at GSI using a newly commissioned time-of-flight diagnostic. The expected energy resolution of the upcoming data should enable a first-time test of the stopping theories in the low-velocity regime of the stopping-power maximum.

ACKNOWLEDGMENTS

This work was supported by the Fonds de Coopération Interrégionale between the Région Aquitaine and the Land Hessen as well as by Bundesministerium für Bildung und Forschung (BMBF), and the Helmholtz International Center for FAIR (HIC4FAIR).

[1] P. Sigmund, *Particle Penetration and Radiation Effects: General Aspects and Stopping of Swift Point Charges*, Vol. 151 in Springer Series in Solid-State Sciences (Springer-Verlag, Berlin, 2006).
[2] D. Schardt, T. Elsässer, and D. Schulz-Ertner, Rev. Mod. Phys. **82**, 383 (2010).
[3] N. Bohr, Phil. Mag. **25**, 10 (1913).
[4] H. Bethe, Ann. Phys. **397**, 325 (1930).
[5] F. Bloch, Ann. Phys. **408**, 285 (1933).
[6] W. H. Barkas, J. N. Dyer, and H. H. Heckman, Phys. Rev. Lett. **11**, 138 (1963).
[7] J. Lindhard, M. Scharff, and H. Schiøtt, Dan. Vidensk. Selsk. Mat. Fys. Medd. **33**, 14 (1963).
[8] G. Maynard, G. Zwicknagel, C. Deutsch, and K. Katsonis, Phys. Rev. A **63**, 052903 (2001).
[9] P. L. Grande and G. Schiwietz, Nucl. Instrum. Methods B **195**, 55 (2002).
[10] P. Sigmund and A. Schinner, Nucl. Instrum. Methods B **195**, 64 (2002).
[11] P. Sigmund, R. Bimbot, H. Geissel, H. Paul, and A. Schinner,, *Stopping of ions heavier than helium*, ICRU Report, Vol. 73 (Oxford University Press, Oxford, 2005).
[12] H. Paul, http://www.exphys.uni-linz.ac.at/stopping/.
[13] H. Paul, Nucl. Instrum. Methods B **247**, 166 (2006).
[14] D. A. Callahan-Miller and M. Tabak, Phys. Plasmas **7**, 2083 (2000).
[15] A. Pelka, G. Gregori, D. O. Gericke, J. Vorberger, S. H. Glenzer, M. M. Günther, K. Harres, R. Heathcote, A. L. Kritcher, N. L. Kugland, B. Li, M. Makita, J. Mithen, D. Neely, C. Niemann, A. Otten, D. Riley, G. Schaumann, M. Schollmeier, An. Tauschwitz, and M. Roth, Phys. Rev. Lett. **105**, 265701 (2010).
[16] T. G. White, J. Vorberger, C. R. D. Brown, B. J. B. Crowley, P. Davis, S. H. Glenzer, J. W. O. Harris, D. C. Hochhaus, S. Le Pape, T. Ma, C. D. Murphy, P. Neumayer, L. K. Pattison, S. Richardson, D. O. Gericke, and G. Gregori, Sci. Rep. **2**, 889 (2012).
[17] A. Golubev, M. Basko, A. Fertman, A. Kozodaev, N. Mesheryakov, B. Sharkov, A. Vishnevskiy, V. Fortov, M. Kulish, V. Gryaznov, V. Mintsev, E. Golubev, A. Pukhov, V. Smirnov, U. Funk, S. Stoewe, M. Stetter, H.-P. Flierl, D. H. H. Hoffmann, J. Jacoby, and I. Iosilevski, Phys. Rev. E **57**, 3363 (1998).
[18] D. H. H. Hoffmann, R. Bock, A. Y. Faenov, U. Funk, M. Geissel, U. Neuner, T. A. Pikuz, F. Rosmej, M. Roth, W. Süß, N. Tahir, and A. Tauschwitz, Nucl. Instrum. Methods B **161**, 9 (2000).
[19] T. Winkler, K. Beckert, F. Bosch, H. Eickhoff, B. Franzke, F. Nolden, H. Reich, B. Schlitt, and M. Steck, Nucl. Instrum. Methods A **391**, 12 (1997).
[20] S. Hayakawa and K. Kitao, Prog. Theor. Phys. **16**, 139 (1956).
[21] A. Ferrari, Annu. Rev. Astron. Astrophys. **36**, 539 (1998).
[22] G. S. Fraley, E. J. Linnebur, R. J. Mason, and R. L. Morse, Phys. Fluids **17**, 474 (1974).
[23] K. Long and N. Tahir, Nucl. Fusion **26**, 555 (1986).
[24] J. D'Avanzo, M. Lontano, E. Tome', and P. F. Bortignon, Nucl. Fusion **35**, 210 (1995).
[25] A. M. Oparin, S. I. Anisimov, and J. Meyer-Ter-Vehn, Nucl. Fusion **36**, 443 (1996).
[26] D. D.-M. Ho, J. A. Harte, and M. Tabak, Nucl. Fusion **35**, 1125 (1995).
[27] M. Roth, T. E. Cowan, M. H. Key, S. P. Hatchett, C. Brown, W. Fountain, J. Johnson, D. M. Pennington, R. A. Snavely, S. C. Wilks, K. Yasuike, H. Ruhl, P. Pegoraro, S. V. Bulanov, E. M. Campbell, M. D. Perry, and H. Powell, Phys. Rev. Lett. **86**, 436 (2001).
[28] J. C. Fernández, B. J. Albright, F. N. Beg, M. E. Foord, B. M. Hegelich, J. J. Honrubia, M. Roth, R. B. Stephens, and L. Yin, Nucl. Fusion **54**, 054006 (2014).
[29] R. Cabrera-Trujillo, P. Apell, J. Oddershede, and J. Sabin, AIP Conference Proceedings **680**, 86 (2003).
[30] D. O. Gericke and M. Schlanges, Phys. Rev. E **60**, 904 (1999).
[31] D. O. Gericke and M. Schlanges, Phys. Rev. E **67**, 037401 (2003).
[32] T. Peter and J. Meyer-ter-Vehn, Phys. Rev. A **43**, 1998 (1991).
[33] D. O. Gericke, M. S. Murillo, and M. Schlanges, Phys. Rev. E **65**, 036418 (2002).
[34] N. Bohr, Dan. Vidensk. Selsk. Mat. Fys. Medd. **18**, 8 (1948).
[35] G. Zwicknagel, Phys. Rep. **309**, 117 (1999).
[36] D. H. H. Hoffmann, K. Weyrich, H. Wahl, D. Gardés, R. Bimbot, and C. Fleurier, Phys. Rev. A **42**, 2313 (1990).
[37] K.-G. Dietrich, D. H. H. Hoffmann, E. Boggasch, J. Jacoby, H. Wahl, M. Elfers, C. R. Haas, V. P. Dubenkov, and A. A. Golubev, Phys. Rev. Lett. **69**, 3623 (1992).
[38] M. Roth, C. Stöckl, W. Süß, O. Iwase, D. O. Gericke, R. Bock, D. H. H. Hoffmann, M. Geissel, and W. Seelig, Europhys. Lett. **50**, 28 (2000).
[39] A. Frank, A. Blažević, V. Bagnoud, M. M. Basko, M. Börner, W. Cayzac, D. Kraus, T. Heßling, D. H. H. Hoffmann, A. Ortner, A. Otten, A. Pelka, D. Pepler, D. Schumacher, An. Tauschwitz, and M. Roth, Phys. Rev. Lett. **110**, 115001 (2013).
[40] C. Deutsch, G. Maynard, M. Chabot, M. Gardes, S. Della-Negra, R. Bimbot, M. F. Rivet, C. Fleurier, C. Couillaud, D. H. H. Hoffmann, H. Wahl, K. Weyrich, O. N. Rosmej, N. A. Tahir, J. Jacoby, M. Ogawa, Y. Oguri, J. Hasegawa, B. Y. Sharkov, A. A. Golubev, A. Fertman, V. E. Fortov, and V. Mintsev, Open Plasma Phys. J. **3**, 88 (2010).
[41] G. Maynard and C. Deutsch, J. Physique **46**, 1113 (1985).
[42] A. B. Zylstra, J. A. Frenje, P. E. Grabowski, C. K. Li, G. W. Collins, P. Fitzsimmons, S. Glenzer, F. Graziani, S. B. Hansen, S. X. Hu, M. G. Johnson, P. Keiter, H. Reynolds, J. R. Rygg, F. H. Séguin, and R. D. Petrasso, Phys. Rev. Lett. **114**, 215002 (2015).
[43] D. J. Edie, J. Vorberger, S. Rose, and D. O. Gericke, EPJ Web of Conferences **59**, 5018 (2013).
[44] HED Properties and Processes, in Workshop on the Science of Fusion Ignition on NIF (2012), https://lasers.llnl.gov/

workshops/science_of_ignition/pdfs/science_of_fusion_ignition_on_NIF.pdf.
[45] O. A. Hurricane, D. A. Callahan, D. T. Casey, P. M. Celliers, C. Cerjan, E. L. Dewald, T. R. Dittrich, T. Döppner, D. E. Hinkel, L. F. B. Hopkins, J. L. Kline, S. Le Pape, T. Ma, A. G. Macphee, J. L. Milovich, A. Pak, H.-S. Park, P. K. Patel, B. A. Remington, J. D. Salmonson, P. T. Springer, and R. Tommasini, Nature (London) **506**, 343 (2014).
[46] J. Jacoby, D. H. H. Hoffmann, W. Laux, R. W. Müller, H. Wahl, K. Weyrich, E. Boggasch, B. Heimrich, C. Stöckl, H. Wetzler, and S. Miyamoto, Phys. Rev. Lett. **74**, 1550 (1995).
[47] D. G. Hicks, C. K. Li, F. H. Séguin, A. K. Ram, J. A. Frenje, R. D. Petrasso, J. M. Soures, V. Y. Glebov, D. D. Meyerhofer, S. Roberts, C. Sorce, C. Stöckl, T. C. Sangster, and T. W. Phillips, Phys. Plasmas **7**, 5106 (2000).
[48] D. A. Pepler, C. N. Danson, R. Bann, I. N. Ross, R. M. Stevenson, M. J. Norman, M. Desselberger, and O. Willi, Proc. SPIE **1870**, 76 (1993).
[49] M. M. Basko, J. Maruhn, and A. Tauschwitz, J. Comput. Phys. **228**, 2175 (2009).
[50] A. Tauschwitz, M. Basko, A. Frank, V. Novikov, A. Grushin, A. Blazevic, M. Roth, and J. A. Maruhn, High Energy Density Phys. **9**, 158 (2013).
[51] M. R. Zaghloul, M. A. Bourham, and J. M. Doster, J. Phys. D: Appl. Phys. **33**, 977 (2000).
[52] A. F. Nikiforov, V. G. Novikov, and V. B. Uvarov, *Quantum-Statistical Models of Hot Dense Matter: Methods for Computation Opacity and Equation of State* (Birkhäuser Verlag, Basel, Switzerland, 2005).
[53] M. Börner, J. Fils, A. Frank, A. Blažević, T. Hessling, A. Pelka, G. Schaumann, A. Schökel, D. Schumacher, M. M. Basko, J. Maruhn, A. Tauschwitz, and M. Roth, Rev. Sci. Instrum. **83**, 043501 (2012).
[54] T. Peter and J. Meyer-ter-Vehn, Phys. Rev. A **43**, 2015 (1991).
[55] D. Vernhet, L. Adoui, J. P. Rozet, K. Wohrer, A. Chetioui, A. Cassimi, J. P. Grandin, J. M. Ramillon, M. Cornille, and C. Stephan, Phys. Rev. Lett. **79**, 3625 (1997).
[56] A. Blazevic, H. G. Bohlen, and W. von Oertzen, Nucl. Instrum. Methods B **190**, 64 (2002).
[57] K. Harres, D. H. H. Hoffmann, R. Knobloch-Maas, F. Nürnberg, A. Pelka, G. Schaumann, M. Schollmeier, A. Schökel, D. Schumacher, J. Schütrumpf, T. Heßling, P. G. Kuznetsov, V. V. Vatulin, O. A. Vinokurov, G. Schiwietz, P. L. Grande, and M. Roth, Phys. Rev. E **81**, 026401 (2010).
[58] A. Ortner, A. Frank, A. Blažević, and M. Roth, Phys. Rev. E **91**, 023104 (2015).
[59] J. P. Rozet, D. Vernhet, and C. Stéphan, Nucl. Instrum. Methods B **107**, 67 (1996).
[60] G. S. Khandelwal, B.-H. Choi, and E. Merzbacher, Atom. Data **1**, 103 (1969).
[61] W. E. Meyerhof, R. Anholt, J. Eichler, H. Gould, C. Munger, J. Alonso, P. Thieberger, and H. E. Wegner, Phys. Rev. A **32**, 3291 (1985).
[62] Bethe and Salpeter, *Quantum Mechanics of One- and Two-Electron Atoms* (Academic Press, New York, 1957).
[63] H. Suno and T. Kato, At. Data Nucl. Data Tables **92**, 407 (2006).
[64] T. Peter, MPQ-Report 105 (1985), http://www.mpq.mpg.de/4464435/mpq_reports#1985.
[65] G. Schiwietz and P. L. Grande, Nucl. Instrum. Methods B **175**, 125 (2001).
[66] C.-K. Li and R. D. Petrasso, Phys. Rev. Lett. **70**, 3059 (1993).
[67] A. Blazevic, B. Rethfeld, and D. Hoffmann, Mat. fys. Medd. **52**, 109 (2006).
[68] H. D. Betz, in *Applied Atomic Collision Physics, Volume 4: Condensed Matter*, edited by S. Datz (Academic Press New York, 1983), p. 2.
[69] D. O. Gericke, Laser Part. Beams **20**, 471 (2002).
[70] J. F. Ziegler, M. D. Ziegler, and J. P. Biersack, Nucl. Instrum. Methods B **268**, 1818 (2010).
[71] H.-K. Chung, M. H. Chen, W. L. Morgan, Y. Ralchenko, and R. W. Lee, High Energy Density Phys. **1**, 3 (2005).
[72] R. Balescu, Phys. Fluids **3**, 52 (1960).
[73] A. Lenard, Ann. Phys. **10**, 390 (1960).
[74] J. Lindhard, Dan. Vidensk. Selsk. Mat. Fys. Medd. **28**, 8 (1954).
[75] S. Skupsky, Phys. Rev. A **16**, 727 (1977).
[76] J. M. Pitarke, R. H. Ritchie, P. M. Echenique, and E. Zaremba, Europhys. Lett. **24**, 613 (1993).
[77] S. Chandrasekhar, Rev. Mod. Phys. **15**, 1 (1943).
[78] N. M. Hoffman and C. L. Lee, APS Meeting Abstracts (2001), p. 2012, http://adsabs.harvard.edu/abs/2001APS..DPPFO2012H.
[79] K. Morawetz and G. Röpke, Phys. Rev. E **54**, 4134 (1996).
[80] G. Maynard, C. Deutsch, K. Dimitriou, K. Katsonis, and M. Sarrazin, Nucl. Instrum. Methods B **195**, 188 (2002).
[81] P. Danielewicz, Ann. Phys. **152**, 239 (1984).
[82] D. Kremp, M. Schlanges, and T. Bornath, J. Stat. Phys. **41**, 661 (1985).
[83] H. A. Gould and H. E. Dewitt, Phys. Rev. **155**, 68 (1967).
[84] D. O. Gericke, M. Schlanges, and W. D. Kraeft, Phys. Lett. A **222**, 241 (1996).
[85] L. S. Brown, D. L. Preston, and R. L. Singleton, Jr., Phys. Rep. **410**, 237 (2005).
[86] R. L. Singleton, Jr., J. Phys.: Conf. Ser. **112**, 022034 (2008).
[87] R. L. Singleton Jr., Phys. Plasmas **15**, 056302 (2008).
[88] Z. Wang, Z.-G. Fu, and P. Zhang, Phys. Plasmas **21**, 102307 (2014).